Engineering Structures 259 (2022) 114181

Contents lists available at ScienceDirect

Engineering Structures

journal homepage: www.elsevier.com/locate/engstruct

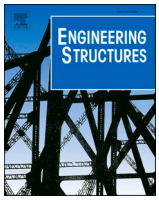

Experimental study on the structural performance of full-scale tyre wall for residential housing applications

Yachong Xu [a], Martin Freney [b], Reza Hassanli [a,*], Yan Zhuge [a], Md. Mizanur Rahman [a], Md. Rajibul Karim [a]

[a] University of South Australia, UniSA STEM, Mawson Lakes, SA 5095, Australia
[b] University of South Australia, UniSA Creative, Adelaide, SA 5000, Australia

ARTICLE INFO

Keywords:
Earthship
Scrap tyre
Tyre wall
Load-bearing wall
Out-of-plane
Full-scale testing
Tyre-encased-soil element

ABSTRACT

End-of-life (EOL) tyres infilled with compacted soil can form segmental tyre-encased-soil elements (TESEs) with considerable load-bearing capacity. The TESEs can be laid course by course in a staggered manner similar to masonry walls to build a load-bearing structure, namely tyre walls. Tyre walls, commonly used in Earthship housing constructions, proved to offer numerous environmental and economic benefits as EOL tyres are effectively upcycled and soil is a widely available and environmentally friendly construction material. However, these walls have been designed based on experience, and there are no certified design guidelines or code provisions available for such systems. Insufficient understanding of the structural performance of tyre walls restrict further applications. This study investigated the structural performance of a tyre wall by conducting experimental tests on a large-scale model. Both axial and horizontal loads were applied. The wall was loaded axially to simulate the roof load before it was subjected to incrementally increasing cyclic out-of-plane load applied at the wall's mid-height. The wall's hysteresis load–displacement response and other key behavioural parameters were studied. The influence of vertical compressive load on the wall's out-of-plane capacity was also investigated. Results revealed that the tyre wall has a linear elastic vertical compressive load–displacement response, and an inelastic out-of-plane load–displacement performance. The out-of-plane failure of the tyre wall was characterized by a joint rotation opening mechanism at the wall's mid-height. "Fat" force–displacement hysteresis curve indicated the tyre wall could perform well in the case of seismic events. The increment of the vertical compressive load had small impact on the tyre wall's out-of-plane performance. Analytical approaches based on the stability of the wall were proposed for calculating the out-of-plane resistance and the results agreed reasonably well with the observed experimental results. This research concluded that tyre walls can be used as structural members for residential housing constructions.

1. Introduction

The number of end-of-life (EOL) tyres is increasing rapidly worldwide. Evidence shows that more than 50 million tyre equivalent passenger units are produced each year in Australia alone, and more than 53.5% of these tyres are stockpiled or illegally dumped [1]. On a global scale, the number of EOL tyres is estimated at 1.5 billion [2]. The stockpiles and dumps of EOL tyres, associated with serious health, environmental and economic problems, have become a public nuisance [3–5]. EOL tyres reused as construction materials in engineering projects have been regarded as possible options to modify some of the mechanical performance of asphalt and concrete products [6–10] and reinforce geotechnical structures [11–20]. Compared with EOL tyres' application in crumbled or shredded forms, using whole tyres helps save processing energy and concomitant greenhouse gas emissions; essentially it is a form of reuse rather than recycling.

Earthships are sustainable residential houses built with natural and waste materials, such as soil and EOL tyres [21–23]. EOL tyres can provide lateral encasement to the infill materials, increase the stiffness and bearing capacity [19,24–27], and form a tyre-encased-soil element (TESE). The TESEs can then be assembled in a running-bond, similar to masonry walls, to form a load-bearing retaining wall structure (tyre wall), a typical feature of the Earthship's earth-sheltered design. The bottom of the tyre wall is embedded into ground while the top is tied to a

* Corresponding author.
E-mail address: Reza.Hassanli@unisa.edu.au (R. Hassanli).

https://doi.org/10.1016/j.engstruct.2022.114181
Received 13 June 2021; Received in revised form 1 January 2022; Accepted 20 March 2022
Available online 26 March 2022

bond beam using either steel bars or straps [21]. Because of the substantial width (585–775 mm) and resilient properties of steel-belted rubber tyres, the tyre walls constructed of TESEs usually do not require steel-reinforced-concrete footings, resulting in both environmental and economic benefits throughout the life-cycle of the house [22].

Tyre walls have been used as load-bearing walls in Earthship constructions in Haiti [28], India [29], the UK [30], the US [21] and Australia [31], as well as the community school in Guatemala [32]. Most of these projects demonstrate that tyre wall construction is applicable in different regions of the world, and results in a lower cost than using manufactured materials in developing countries [32]. As tyre walls incorporate large quantities of thermal mass into the building envelope, when combined with passive solar design principles, it results in a home that requires little to no energy to heat and cool. The study performed by Freney, Soebarto [22] revealed that tyre walls with rigid insulation cladding are comparable in thermal performance to straw bale walls and when an earth berm is combined with a tyre wall to create an earth-sheltered home, heating and cooling energy is negligible in temperate climates. The thermal mass of the tyre wall and the earth-sheltering method create a thermal flywheel effect that naturally regulates the indoor air temperature in a wide variety of climates [22,30,31,33–36]. Therefore, the tyre-wall "Earthship" houses proved successful in architectural behaviours and structural stability. It is predicted that the tyre walls would have a broader application in the future, especially in countries where labour costs are low, and mechanisation is limited; however, in developed countries, systems for mechanising the process have been developed [37]. Despite several thousand tyre-wall Earthships having been built worldwide relying on engineers' experience [21,30,31,38], insufficient understanding of the structural performance restricts further application of tyre walls. Although some previous research work has been completed evaluating the structural performance of tyre walls [39,40], there is a general scarcity of high-quality data and analysis techniques that can be used to design such walls. Therefore, more studies on such structures are required to be able to systematically and safely design and use such walls as structural load-bearing members.

The fundamental focus of this research project is the experimental and analytical evaluation of the out-of-plane performance of tyre walls subjected to one-way bending. These aspects were targeted to explore the wall's ability to resist the forces resulting from the retaining wall application (backfilling the wall for earth-sheltering). Experimental tests designed, carried out and reported here on a full-scale tyre wall aimed at studying the structural performance, including vertical compressive stiffness, out-of-plane cyclic hysteresis load–displacement responses and failure mode of such walls. The effect of vertical compressive load (which simulates the roof load) on the tyre wall's out-of-plane performance was also a focus of this study. Analytical approaches for calculating the out-of-plane resistance derived based on the stability of the wall were developed and compared with the observed testing results.

2. Experimental program

The experimental work was divided in three stages. In *Stage I*, pure axial compressive load was applied to the wall to simulate the compressive performance of the wall subjected to roof load. In *Stage II*, the axial force was maintained, and out-of-plane load cycles with increasing magnitude was applied at the tyre wall's mid-height to investigate the hysteresis load–displacement response of the wall under out-of-plane loading. In the *Stage III*, the wall was subjected to four sets of out-of-plane cycles of imposed displacement with four different axial compressive loading to investigate the effect of axial force on the wall's out-of-plane performance. Detailed description regarding the construction materials, design and construction procedures of the test specimen, test setup and loading regimes are presented in the following subsections.

2.1. Material characterization

2.1.1. Soil

Sandy loam sourced from a local supplier in Adelaide, South Australia was used to build the tyre wall in this study. The particle size distribution (PSD) of the sandy loam was determined through standard sieve analysis following AS 1289.3.6.1 [41]. The PSD is presented in Fig. 1. According to the Unified Soil Classification System (USCS) [42], the soil was classified as poorly graded sand (SP) and had uniformity coefficient (C_u) of 3.3 and curvature coefficient (C_c) of 1.0. Standard compaction tests were performed following AS 1218.5.1.1 [43]. The optimum moisture content (OMC) and maximum dry density (MDD) values were 12.5% and 1700 kg/m^3, respectively. Sandy loam was used because it is commonly available worldwide as garden soil, and it is the cheapest soil that can be easily obtained from the local soil market. Changing the soil type changes the stiffness of TESEs accordingly due to the variance in soils' characteristics. For example, the encased soil with a higher cohesion and friction angle would induce a higher elastic modulus to the TESEs.

2.1.2. Tyre

EOL 175/65R14 tyres provided by a national tyre recycler, Tyrecycle Pty Ltd. were used to build the tyre wall. The tyres had an outer diameter of 584 mm, a rim diameter of 355.6 mm, and a height (tread width) of 175 mm. Random-brand tyres were selected using a simple visual observation criterion, ie, intact surface with no cord damage (no exposed steel radials). The general physical properties used to characterize the tyre materials, such as the hyper elastic property of the tyre rubber were difficult to obtain, especially for randomly collected EOL tyres. Because tyres are composite materials of rubber, fabric and metallic mesh, the tyres produced by different manufacturer or even within different batches (by the same manufacturer) may have variance in their construction and structures [44–47]. Since the main function of the tyre in TESEs is to provide circumferential confining stress, similar to geocell and geotextile [19,20,48,49], to restrict the movement of the encased soils, the tensile properties of the EOL tyres in the circumferential direction were tested following ASTM D638-14 [50] at a displacement-control rate of 5 mm/min. This method may underestimate the elastic modulus of the tyre material. A commercial laser cutting service was employed to cut two tensile specimens (Type I specimen as described in the standard) from each tyre tread in the circumferential direction. The average thickness of the specimens was 11.9 mm, and other dimensions are shown in Fig. 2. The tensile stress and strain relationships of the specimens are shown in Fig. 2. The average yield stress and yield strain were 14 MPa and 13.1%, respectively. The average elastic modulus was 112 MPa, calculated as the ratio of yield stress to the yield strain.

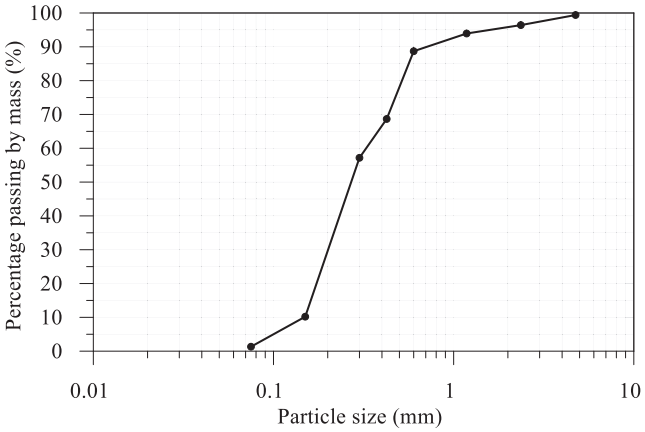

Fig. 1. Particle size distribution (PSD) of the sandy loam (USCS: SP).

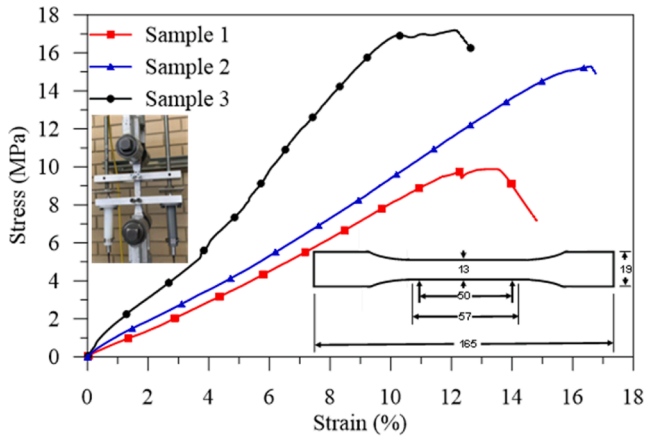

Fig. 2. Tyre tensile test sample (dimensions in mm) and results.

2.2. Design and construction of the test tyre wall

The tested tyre wall had a height of 1858 mm, length of 2855 mm and an average width of 570.7 mm. Australian Building Codes Board [51] stipulated that the required ceiling height for a habitable room in residential houses should be not less than 2400 mm. This study made a compromise to reduce the height of the tyre wall specimen to 1858 mm to ensure experimental safety. Although the height was decreased, the slenderness ratio was maintained by using smaller than "normal" size tyres for an Earthship tyre wall. The slenderness ratio (=height/width) of the test wall was equal to 1858/570.7 = 3.26. The length of a wall is generally determined by the function and required size of a room. This study adopted a wall length of 2855 mm, as a longer wall could not be tested due to the limitation in the laboratory space and equipment. The width of the wall was taken as the outer diameter of the constructed TESEs.

The tyre wall was built by laying nine courses of TESEs in a running bond (similar to dry-stack masonry walls). The construction involved TESEs made with whole and cut tyres. The cut tyres were made by cutting off the steel beads using a portable jigsaw and cut open the tread in the direction perpendicular to the tread (see Fig. 3(a) and (b)). The procedures for constructing the tyre wall comprised of six steps: (1) place EOL tyres horizontally in a line on the wall's location; (2) insert cardboard into the tyres to cover the bottom openings so that the tyres with cardboard can form containers with only one top opening; (3) add soil into the containers and compact; (4) level the top surfaces to ensure they are parallel to each other and the ground surface; (5) lay empty EOL tyres onto the top of the previous course, and repeat step 2 to 5; (6) put cut tyre (as shown in Fig. 3(b)) at the second most end position in alternative courses and connect it to the last whole TESEs using screws, and repeat step 2 to 6 until the wall reaches the final height.

2.3. Test setup

The details of the test setup are presented with the help of CAD drawings (Fig. 4) and pictures (Fig. 5 and Fig. 6). Two strong reaction frames, each containing two strong columns and one strong beam, were employed to provide the reaction force during testing, as shown in Fig. 4 (a) and (b). One axial loading actuator located at the top centre of the wall was clamped to the strong beam to provide axial compressive load to the tyre wall (Fig. 4(a) and Fig. 6(a)). A 3 m long steel I-beam (310 UB 46.2, referred to as "axial loading beam") was placed on top of the tyre wall which allowed even distribution of the axial load and simulated the bond beam (see Fig. 4 and Fig. 5(a)). The axial load was measured using a load cell sensor installed on the actuator. The axial displacement of the tyre wall was measured by two linear variable differential transducers (LVDTs), respectively located at each end of the axial loading beam (Fig. 4(a), Fig. 5(a) and (f)). The result analysis was performed based on an average value recorded by the two axial LVDTs.

In order to maintain safety and avoid a sudden collapse of the wall during testing, the top flange of the axial loading beam was loosely secured to the reaction frame using hanging chains (Fig. 5(a)). The top-course of the TESEs was also secured to the bottom flange of the axial loading beam using loose chains (Fig. 5(d)). This helped to secure the wall during testing and at the same time provided a reasonable degree of freedom to the tyre wall system, so that the experimental results would not be influenced.

Universal Material Testing System (MTS) with a hydraulic actuator of 100 kN load capacity and a maximum stroke of 300 mm was used to apply the out-of-plane lateral loads. The actuator was clamped on the side of the out-of-plane reaction frame at the tyre wall's mid-height. The actuator load was evenly distributed to the wall through a 3.6 m steel I-beam (size 150 UB 18.0, named lateral loading beam in Fig. 4(a) and Fig. 5(a)). The lateral loading beam was weld connected to the head of the actuator. The lateral loading beam was also supported by two end-rails made of steel channels (300 PFC, as shown in Fig. 4(a) and Fig. 5 (c)), which allowed the lateral load to be perpendicular to the wall throughout the test. The frictional resistance due to sliding of lateral loading beam was less than 0.15 kN. The frictional force has been subtracted from the measured result. The lateral displacement of the tyre

Fig. 3. Method of cutting tyres: (a) cut steel beads and cut cross; (b) cut tyre.

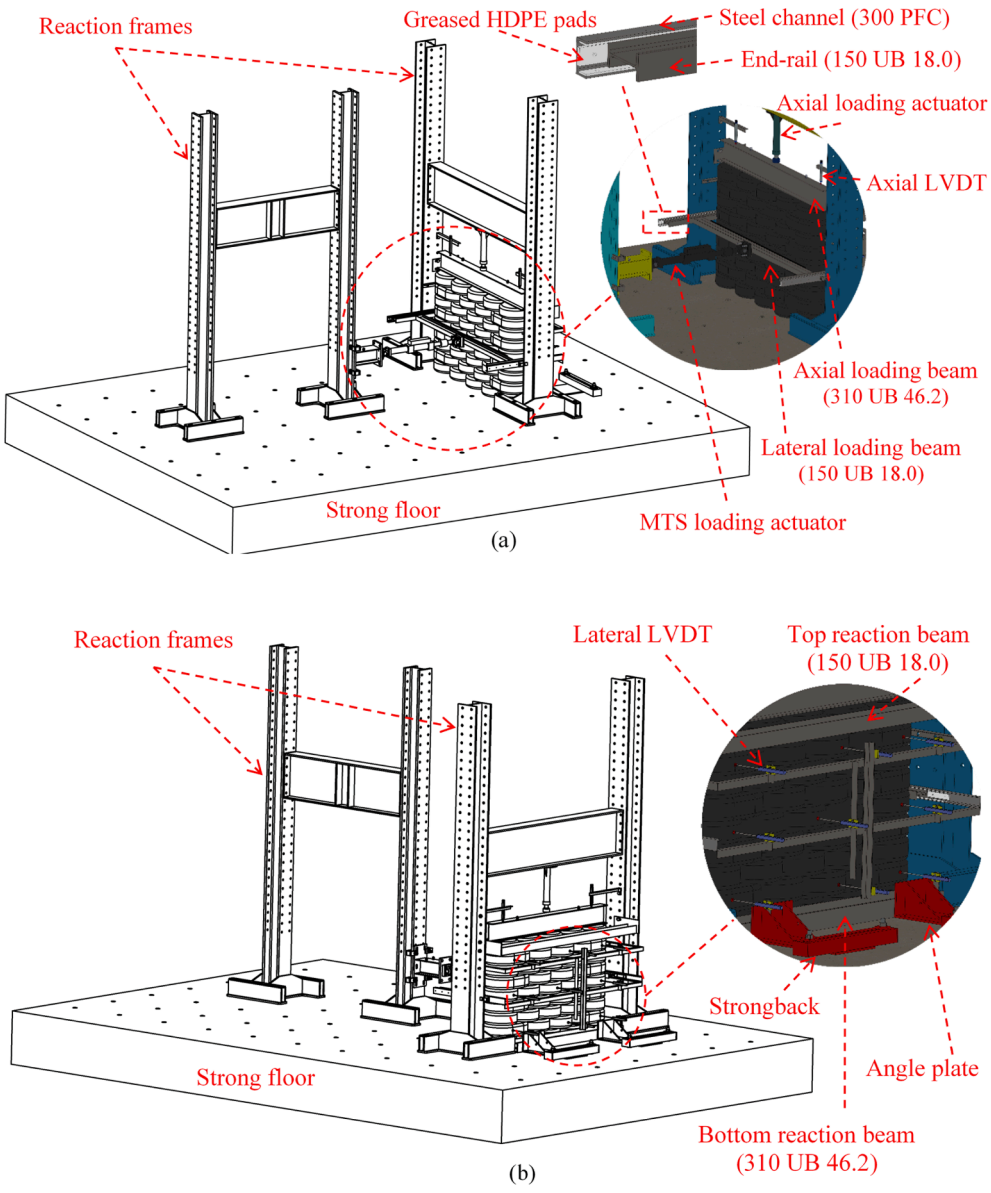

Fig. 4. Test setup CAD drawing: (a) Frontside isometric view; (b) Backside isometric view.

wall was logged using 9 LVDTs located at top, middle and bottom of the wall (Fig. 4(b), Fig. 6(a) and (c)). The 3 row LVDTs were located at heights of 1529 mm, 900 mm, and 285 mm from the ground. Two steel I-beams (150 UB 18.0 on top and 310 UB 46.2 at the bottom) were mounted as the reaction beams at the tyre wall's back to provide one-way supports (Fig. 6(a), (d) and Fig. 4(b)). The top reaction beam was located at the height of the top-course TESEs of the tyre wall, while the bottom reaction beam was fixed on the strong floor.

2.4. Loading regime

The experimental program involved three stages of testing, details of which are presented in the following.

2.4.1. Stage I: Axial compressive loading

The axial compressive force history is shown in Fig. 7. A 100 kN capacity hydraulic actuator with a manual hydraulic pump was employed to apply the axial compressive force from 0 kN to 10 kN. The self-weight of the axial loading beam was 1.4 kN.

2.4.2. Stage II: Combined constant axial compression and cyclic out-of-plane loading

After the *Stage I* compression testing, the axial compressive load was maintained at 10 kN to simulate the typical dead load from a light-weight roof. The axial compressive load was applied using a manual hydraulic pump. The manual hydraulic pump was fitted with a hydraulic flow-control value, which allowed manual intervention on the axial load during the test. The reason for the human intervention was that the axial load might change due to the tyre wall's deflection while testing, but the roof weight is constant in real situations. The fluctuation of the axial compressive force, as shown in Fig. 7, was generated by the wall's axial displacement and the manual intervention on the axial load. Although a degree of fluctuation was measured, the fluctuation of the axial force was mostly kept within 2 kN differences, and the trend of the out-of-plane load–displacement result was not significantly influenced (as shown in Fig. 13).

Since Earthship tyre walls are sheltered with earth, the majority of the lateral loads acting on the wall are due to earth pressure. To simulate forces resulting from active soil pressure at different applied displacement, cyclic loading and unloading protocols suggested by Ghobarah

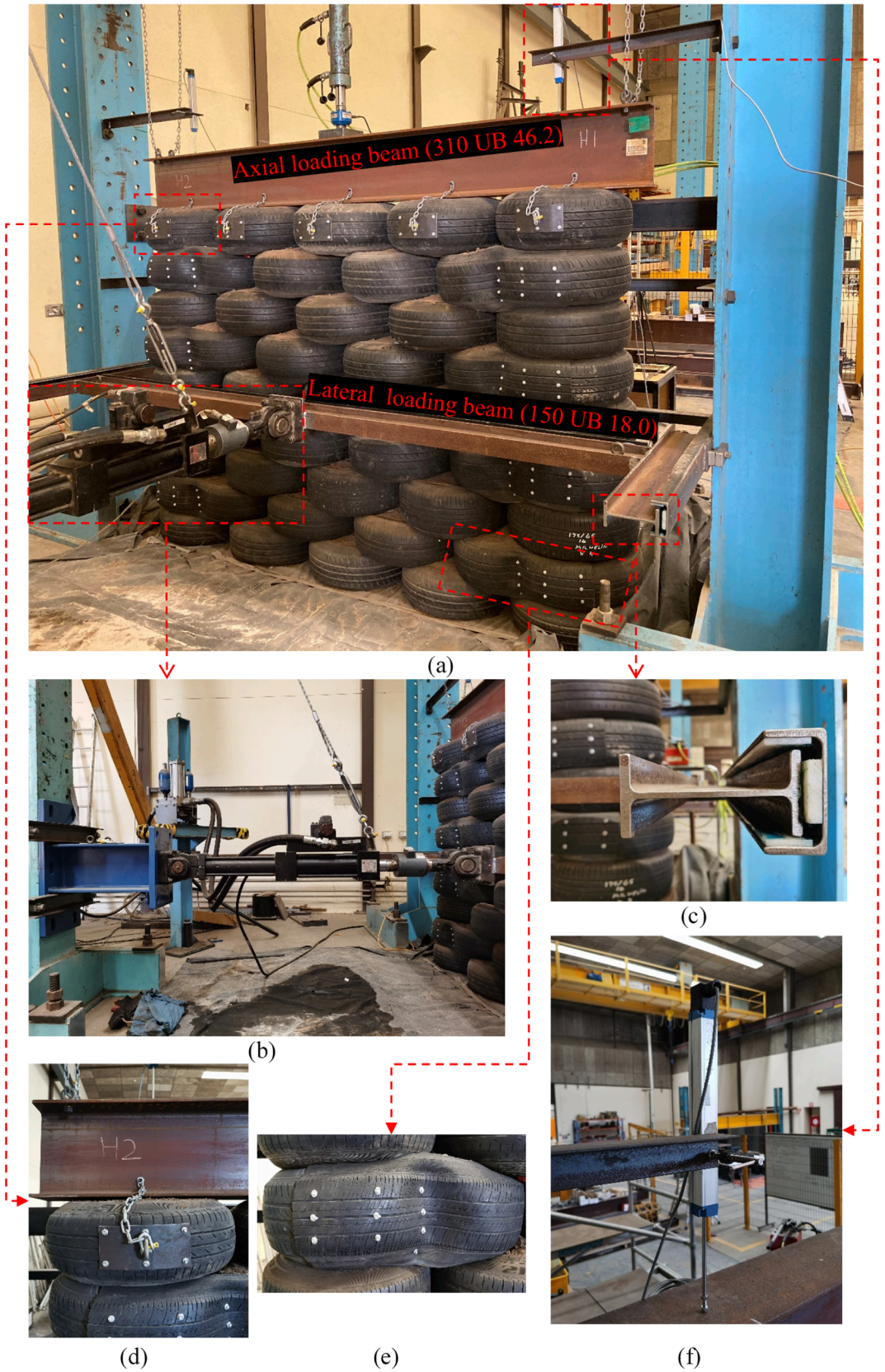

Fig. 5. Front side test setup: (a) overall view; (b) MTS loading machine; (c) lateral loading beam sliding arrangement; (d) safety chain connection between top-course TESEs and axial loading beam; (e) cut tyre connection; (f) Axial LVDT. (Photos b, d, e taken after testing).

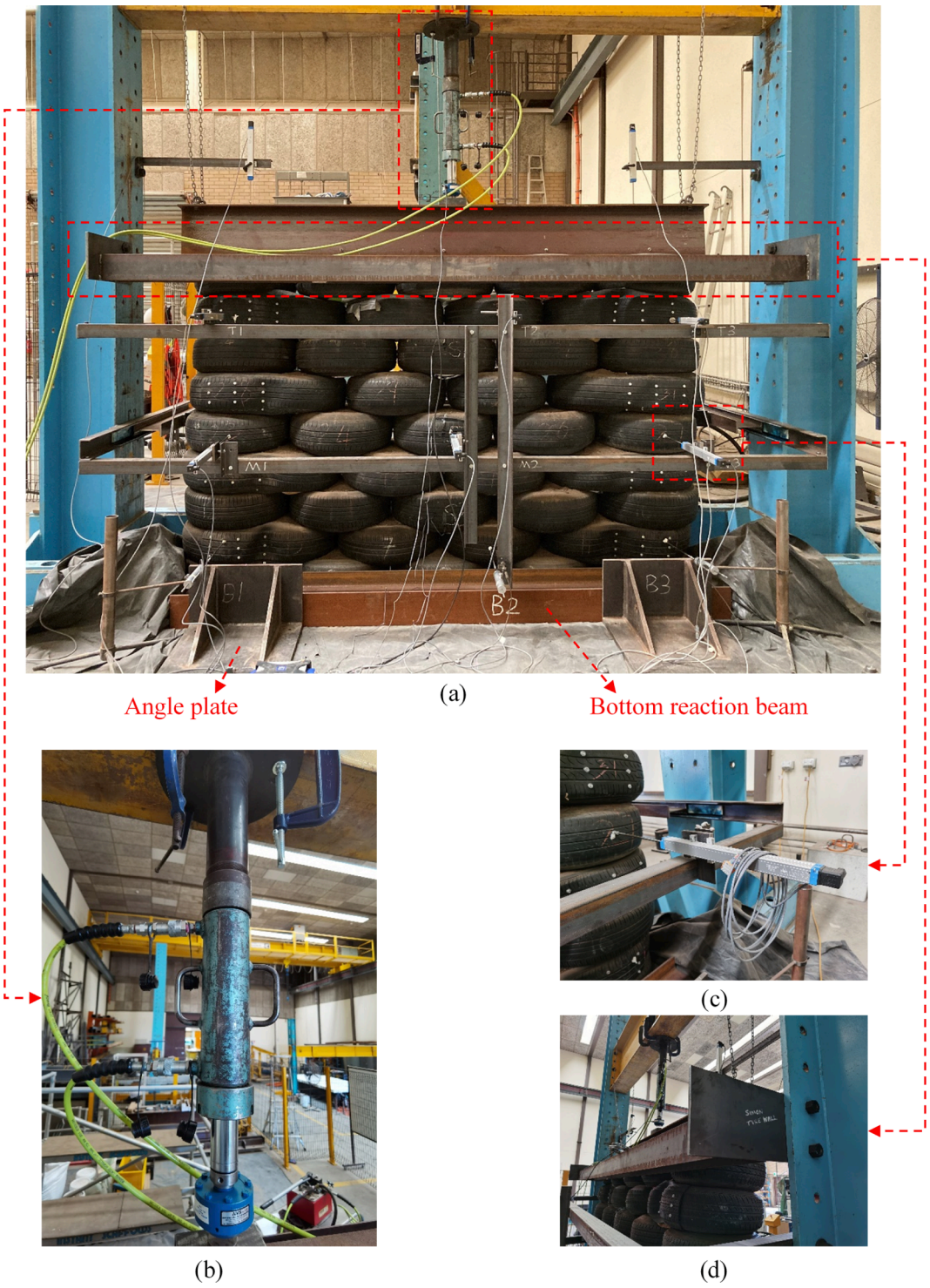

Fig. 6. Backside test setup: (a) overall view; (b) axial loading actuator; (c) lateral LVDT; (d) bolt connection of the top reaction beam with steel plate welded at the end.

and Galal [52] for masonry wall testing was adopted. The loading rate was 0.08 mm/s for the initial five cycles and 0.5 mm/s for the later cycles, as shown in Fig. 8. The cyclic loading regime used in this study was modified in accordance with Test Method B as provided in standard ASTM E2126-11 [53]. The wall was estimated to reach its ultimate out-of-plane displacement (Δ_m) at about 225 mm. The initial five loading-and-unloading cycles were applied to the wall at displacement amplitudes of 1.25%, 2.5%, 5%, 7.5% and 10% of the ultimate displacement (Δ_m), followed by three cycles with amplitude displacement of 20%, 40% and 60% of Δ_m. The original loading plan involved cycles with displacement amplitude of 80%, 100% and 120% of Δ_m. However, for safety reasons, the cyclic loading test was stopped after completing the cycles with a displacement amplitude of 60% Δ_m, when the integrity of the tyre wall was observed to be at risk.

2.4.3. *Stage III: Combined varying axial compression load and out-of-plane loading*

Stage III testing aimed to investigate the effect of axial load on the

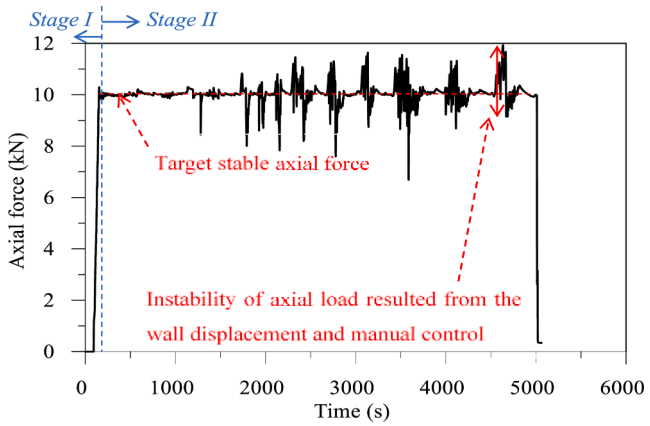

Fig. 7. Axial loading regime in *Stage I* and *Stage II*.

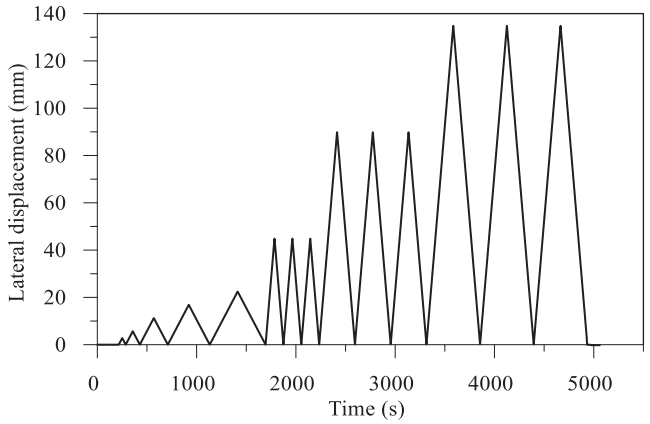

Fig. 8. Out-of-plane loading regime in *Stage II*.

out-of-plane performance of the tyre wall. Fig. 9 and Fig. 10 present the regimes of the axial compressive loads and the out-of-plane loads. The applied axial load aimed to simulate the typical vertical load transferred from the roof to the tyre wall in real scenarios. The typical vertical loads were calculated as the sum of the dead load obtained from Ref. [54] and the live load obtained from Ref. [55], which result could vary from 0.67 kPa for a light-weight wooden roof to 6.5 kPa for a heavy concrete roof. Since residential housing roofs in Australia are generally made of wooden structures with tiles. It is reasonable to assume that the roof (relatively light weight from 1.2 kPa to 4.6 kPa) is one-way supported by tyre walls and with a spanning length of around 3.0 m. Therefore, this

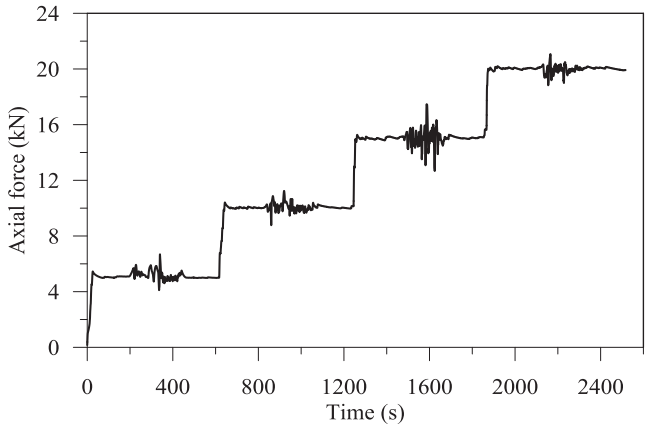

Fig. 9. Axial loading regime in *Stage III*.

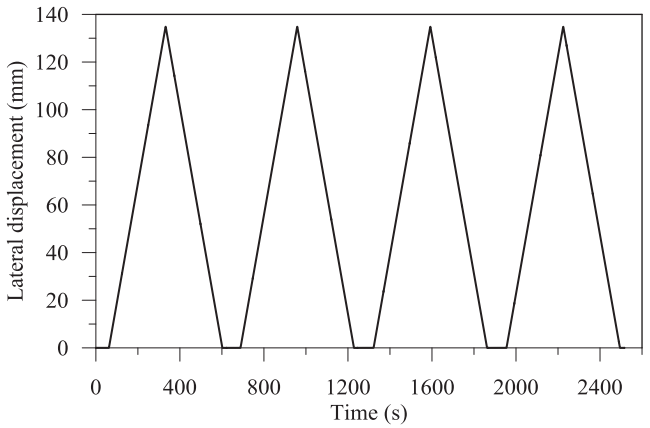

Fig. 10. Out-of-plane loading regime in *Stage III*.

study adopted axial loads from 5 kN to 20 kN with 5 kN increments. A constant 135 mm (=60% of Δ_m) out-of-plane displacement cycle was applied at each axial force level. The loading rate of the out-of-plane displacement was 0.05 mm/s.

3. Experimental results and discussions

The results from each of the stages of testings is provided in the following.

3.1. Stage I: Compressive performance of a tyre wall subjected to pure axial compression

Fig. 11 presents the axial forces plotted against axial displacement. The axial displacement of the tyre wall increased with the increasing axial compressive force. The axial force–displacement relationship approximated a linear trend. At 10 kN compression, the axial displacement of the tyre wall was 3.7 mm (0.2% of the tyre wall's height). The result indicated that tyre walls could be safely used as a load-bearing structural member in residential housing constructions with light-weight roof. The deformable characteristics of the tyre wall prevented it from a brittle failure, which is a typical failure phenomenon observed in compression experiments of traditional masonry brickworks [56].

3.2. Stage II: Cyclic out-of-plane performance of tyre wall subjected to 10 kN axial compressive force

3.2.1. Testing observation and failure mechanism

Tyre wall subjected to combined compressive and out-of-plane

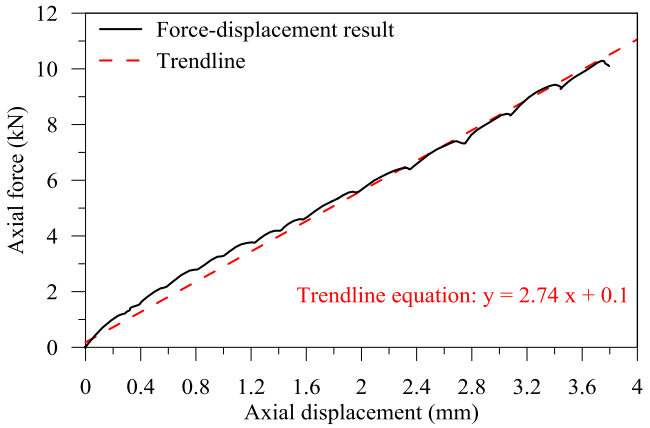

Fig. 11. Axial force–displacement result.

loading was mainly impacted by a joint rotation opening mechanism at the wall's mid-height (Fig. 12), which is also one of the typical failure behaviours of the unreinforced masonry brickworks subjected to one-way vertical bending [56–58]. When out-of-plane loads were applied, the wall at mid-height was displaced in the loading direction with the bottom of the wall showing small movement in the same direction and the wall top displaced in the opposite direction. The tyre wall displayed a bending response characterized by rotation and opening of the interface between the 5th and 6th courses (Fig. 12(a)). The wall also displayed relative shear displacements between courses. The joint opening did not occur exactly at the walls' mid-height. This was due to the load being applied at the middle course of the wall rather than the joint.

Once the out-of-plane loads were removed, the joint rotation opening at the wall's mid-height closed (Fig. 12(b)). The out-of-plane displacement of the wall did not recover back to zero and the residual shear displacement accumulated with the increasing number of loading cycles. The deformed shape of the tyre wall upon cyclic testing is shown in Fig. 12(c). As shown, no failure was found on individual TESEs. No gap was observed between TESEs in the same course in the in-plane direction.

3.2.2. *Out-of-plane force–displacement hysteretic response*

The out-of-plane force–displacement hysteretic response of the wall is presented in Fig. 13. Drift ratio, defined as the out-of-plane displacement divided by the wall's height (1858 mm), was plotted as the secondary x-axis in the figure. The 'fat' force–displacement hysteresis loops demonstrate the tyre wall's cyclic out-of-plane loading behaviour to be highly inelastic, which is beneficial with regard to their seismic performance. The out-of-plane force increased with increasing

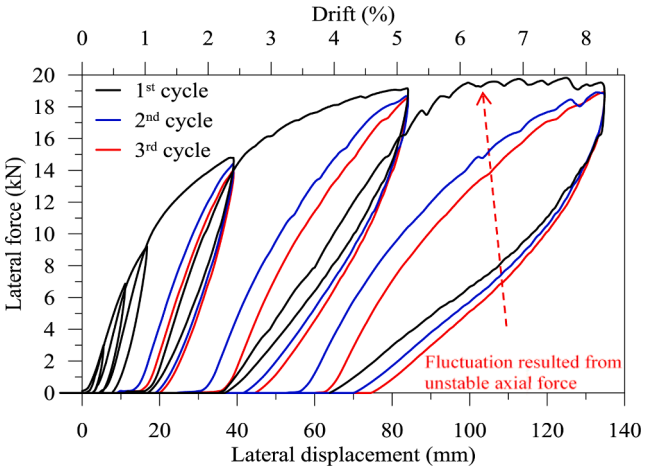

Fig. 13. Lateral force–displacement hysteretic curve (*Stage II*).

out-of-plane displacement but with a lower rate at larger drifts. The out-of-plane force was nearly reaching a plateau after imposed displacement of 90 mm (=4.8% drift ratio). The ultimate force was 19.8 kN at corresponding 120 mm displacement (=6.4% drift ratio). The tyre wall's ability to maintain its ultimate force for displacing another 30 mm distinguish it from the traditional unreinforced masonry brickworks [58,59], thanks to the substantial thickness of the tyre wall section and the deformability of TESEs units. The tested maximum displacement was 135 mm (=7.3% drift ratio) when the test was stopped to avoid

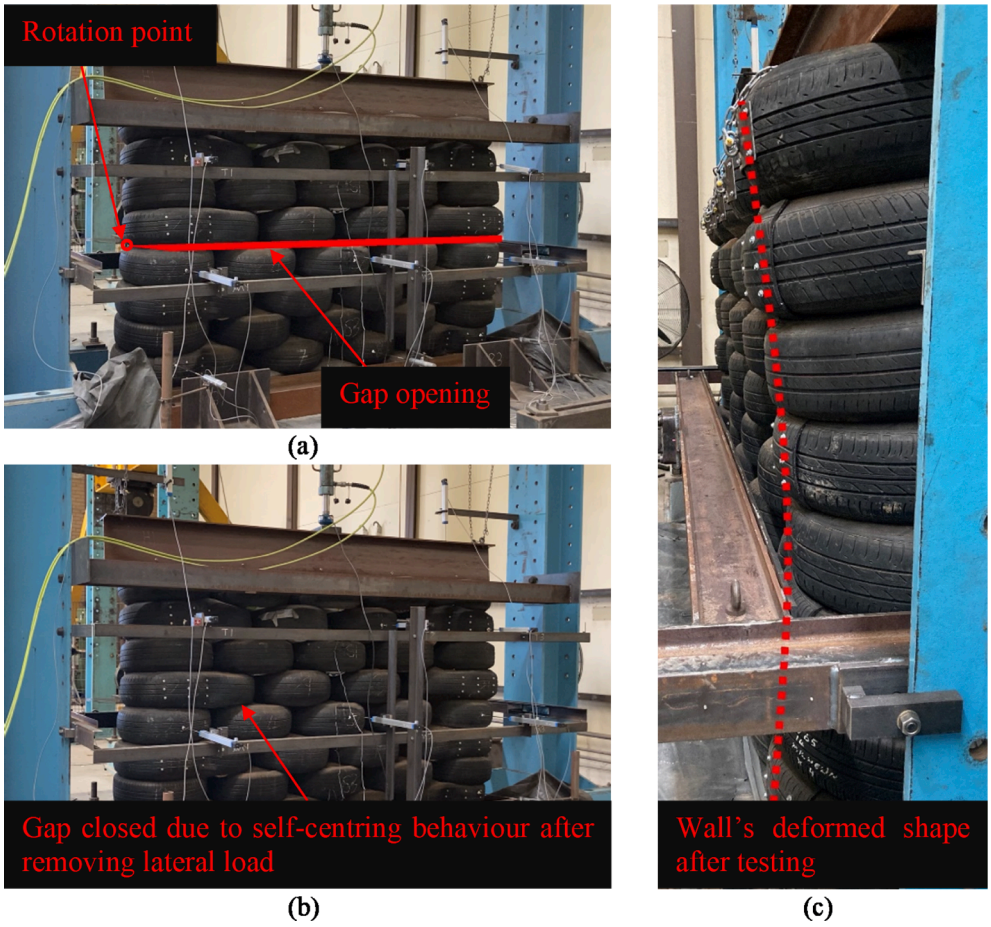

Fig. 12. Failure behaviour: (a) opening of the tyre wall under out-of-plane load; (b) recovery of the tyre wall after removing loads; (c) Tyre wall remained bent after *Stage II* testing.

damaging the testing equipment due to potential wall instability. In real-life applications, a typical load-bearing wall of a residential house with a height of 2.4 m would not have such a high drift ratio (7.3%) to fulfil the serviceability requirements. In most loading and unloading cycles, the peak force point coincided with the point of peak displacement. However, in the first cycle of 60% amplitude, the two points did not coincide due to the fluctuation of the out-of-plane force with increasing displacement. The fluctuation presented in the curves resulted from the instability of axial force (shown in Fig. 7).

3.2.3. Residual out-of-plane displacement

The out-of-plane displacement at the point of zero out-of-plane force after each loading cycle was considered as the residual displacement. The residual displacement was mostly composed of relative shear displacement between the courses of the TESEs and the deflection of the TESEs. The residual displacement increased with the increasing imposed displacement (Fig. 14), which was because the larger imposed displacement induced a greater relative shear displacement between the courses of the TESEs. Without external pulling forces, the potential energy incorporated in the tyre wall was not sufficient to self-centre the tyre wall by recovering the relative shear displacement back to zero. The first cycles of each amplitude generated a larger shear and residual displacement to the tyre wall between courses of TESEs (Fig. 14). The ultimate residual displacement was approximately 75 mm (=4% drift ratio) at the end of the imposed 135 mm-displacement (=7.2% drift ratio) cycles.

3.2.4. Backbone curves, bilinearized curve and ductility

The backbone curve (shown in Fig. 15) displays a non-linear pattern, indicating the tyre wall had a non-linear out-of-plane load–displacement behaviour. The backbone curve was plotted using the coordinates of the envelope points from the lateral force–displacement hysteretic curves (Fig. 13). The lateral force increased with an increasing displacement at a higher rate before the lateral displacement reached 45 mm (=2.4% drift ratio). After this point, the lateral force increased at a slower rate until the end of the test.

The backbone curve of the tyre wall was bilinearized in accordance with the method provided in FEMA 356 [60] to calculate the effective lateral stiffness (K_e) and the effective yield strength (F_y) of the tyre wall system. The bilinearization curve, shown in Fig. 15, is composed of two line segments: one line segment, with slope of K_e, linking the axis origin (Δ_0, F_0) and the effective yield point (Δ_y, F_y), and another line segment linking the effective yield point and the point of ultimate force (Δ_u, F_u). The effective lateral stiffness (K_e) was taken as the secant stiffness calculated using the backbone curve at the out-of-plane force equal to 60% of the effective yield strength (F_y). The coordinate of the effective yield point was located by using iterative graphical procedure to have

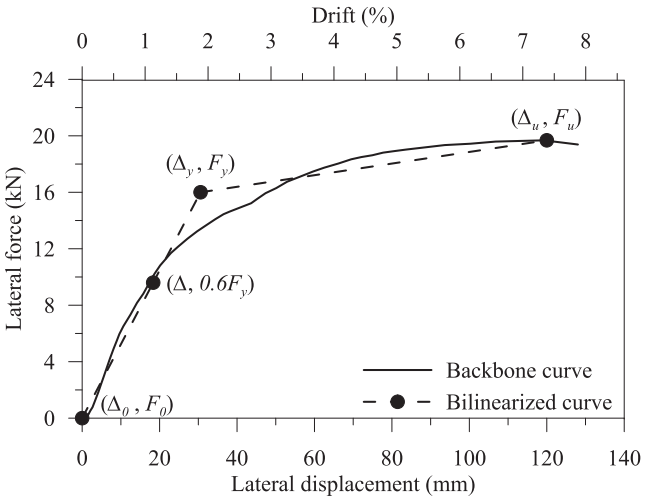

Fig. 15. Backbone curve and bilinear EEEP curve.

balanced areas above and below the backbone curve among the areas enclosed between the two curves. The effective yield strength (F_y) and corresponding yield displacement were 16 kN and 30.6 mm, respectively. The effective lateral stiffness (K_e) was 0.52 kN/mm, calculated as the slope of the elastic portion of the bilinearized curve. The displacement ductility ratio was 4.4, which was calculated as the ratio of the ultimate displacement (135 mm) observed in the cyclic test and the effective yield displacement (30.6 mm) of the tyre wall. The displacement ductility ratio of the tested tyre wall was higher than that of typical unreinforced masonry structures, whose displacement ductility ratio is generally between 1 and 2 [61]. The ductile performance of the tested tyre wall was considered acceptable with respect to seismic resistance.

3.2.5. Lateral stiffness and stiffness degradation

The lateral stiffness was obtained as the secant stiffness (K_s), which was calculated as the slope of the line passing through the origin and the intersecting with the hysteresis loop at the peak force (Δ, F_{max}) points in the 1st cycles, as expressed by Eq. (1):

$$K_s = \frac{F_{max} - F_0}{\Delta - \Delta_0} \tag{1}$$

The secant stiffness at each loading cycle is normalized by the effective lateral stiffness (K_e) at the effective yield displacement. The trends of secant stiffness (K_s) and normalized stiffness (K_s/K_e) in regard to the imposed lateral displacement and the imposed drift ratio, are illustrated in Fig. 16. The results indicated that the wall's load resistance

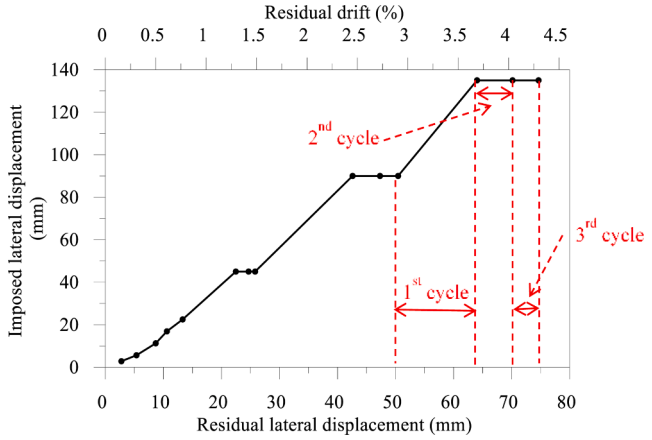

Fig. 14. Imposed lateral displacement vs. residual lateral displacement.

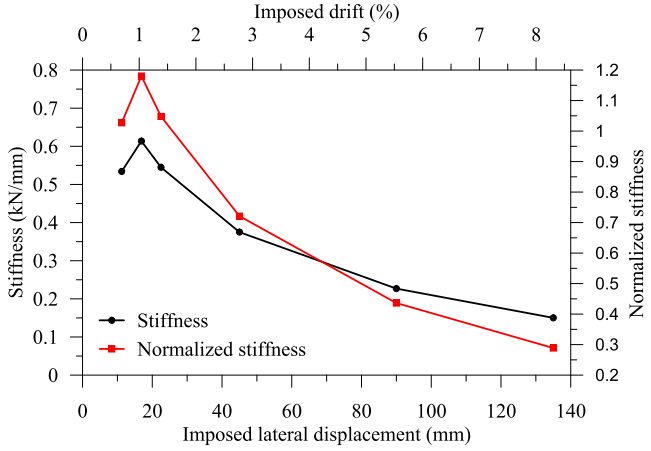

Fig. 16. Stiffness degradation.

increased with increasing displacement for up to lateral displacement of approximately 17 mm (≈1% drift ratio), as indicated by the 19% enhancement in stiffness. The stiffness enhancement was due to densification and hardening of the encased soil, which resulted from the arching effect induced by combined out-of-plane and compressive loading. After that, the tyre wall displayed a non-linear stiffness degradation response. The stiffness degradation of the dry-stack tyre wall was highly impacted by the deformation and residual displacement of the TESEs (as discussed in Section 3.2.3). At ultimate out-of-plane load capacity (19.8 kN, 120 mm), the wall's secant stiffness was approximately 0.16 kN/mm, which was 31% of its yield stiffness.

3.2.6. Energy dissipation

The reverse loading forces were not applied during testing, so the energy dissipation only involves the energy dissipated during loading and unloading processes in the push direction. Fig. 17(a) and (b) present the dissipated energy and cumulative dissipated energy respectively with respect to the imposed lateral displacements. The amount of dissipated energy were calculated as the area enclosed by the first cycle's hysteresis loop at each amplitude (shown in Fig. 13). Fig. 17(a) indicates that prior to 5.8 mm lateral displacement, the energy dissipation resulted from the deformation of tyre rubber and rubber attached to the lateral loading beam was negligible. The evident increment of energy dissipation started from 5.8 mm lateral displacement and increased with increasing imposed lateral displacement. Fig. 17(b) demonstrates that, after 20 mm imposed lateral displacement, the relationship between the cumulative energy dissipation and the amplitude was almost linear. The cumulative energy dissipation reached 1444 J at the corresponding imposed displacement of 135 mm. The energy losses mainly resulted from the residual lateral displacements and the frictional resistance.

3.2.7. Equivalent viscous damping ratio

The equivalent viscous damping ratio (ξ_{eq}) is used to describe the damping behaviour of a system. This parameter can be obtained by equating the stored elastic strain energy (E_s) of the system with the dissipated energy (E_d) during cyclic loading [62]. The equivalent viscous damping ratio of a half cycle can be calculated following Eq. (2):

$$\xi_{eq} = \frac{E_d}{2\pi E_s} \tag{2}$$

Fig. 18 shows the results of equivalent viscous damping ratio plotted against imposed lateral displacement and imposed drift ratio. The results show that the tyre wall had an increasing equivalent damping ratio with the increase in lateral drifts. The damping ratio of the tyre wall varied from around 0.08 at lower drifts to about 0.18 at the drift of about 7.0%.

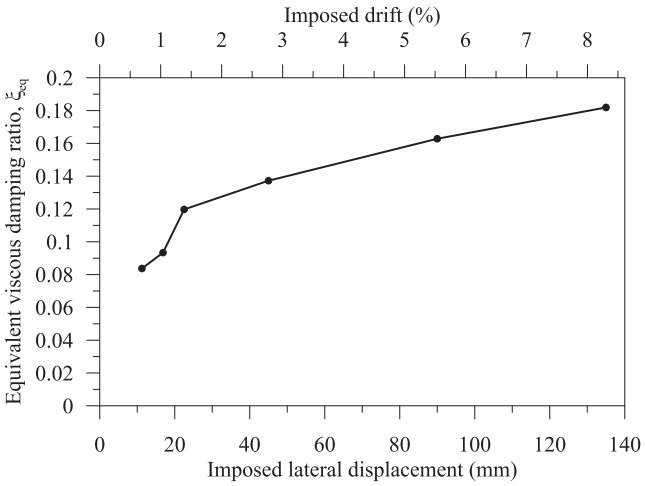

Fig. 18. Equivalent viscous damping ratio versus imposed lateral displacement and imposed drift.

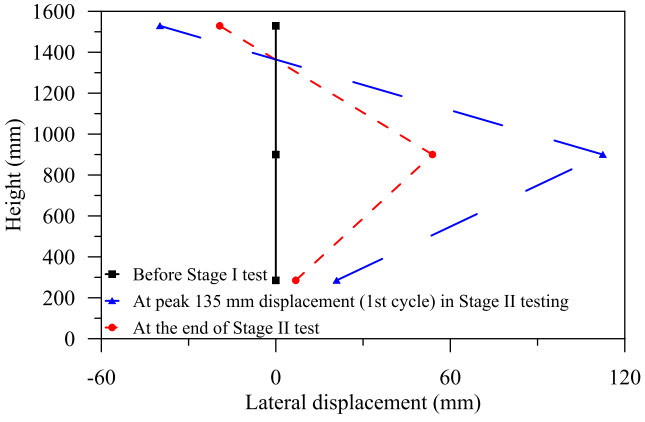

Fig. 19. Wall deformation profile.

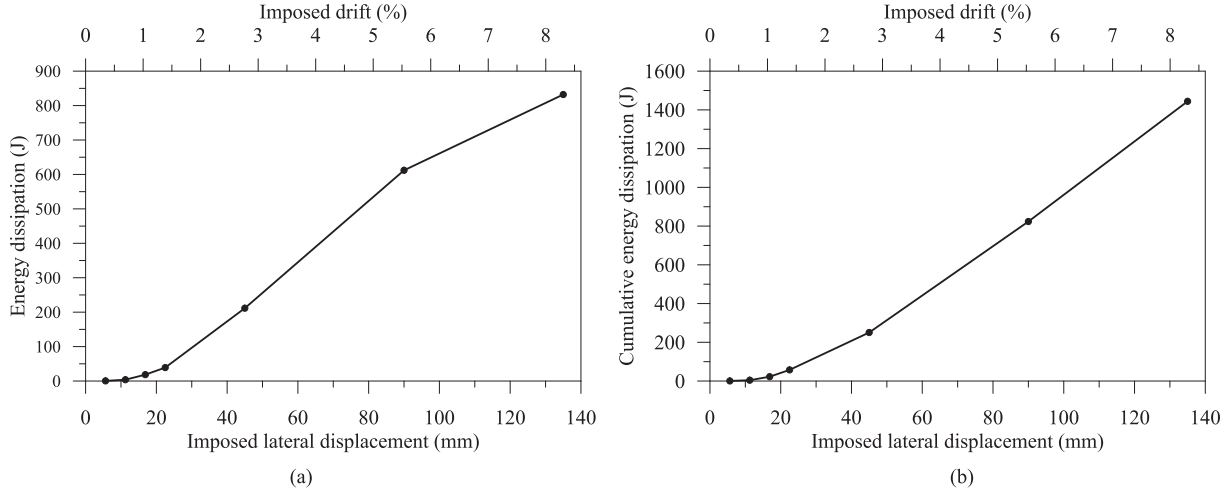

Fig. 17. Energy dissipation during loading and unloading processes: (a) energy dissipation during the first cycle of each amplitude; (b) accumulative energy dissipation of the first cycles of each amplitude.

3.2.8. Wall deformation profile

Fig. 19 shows the wall displacement profile, which includes: (1) the initial lateral displacement of the wall before testing; (2) the lateral displacement of the wall at the first peak movement of 135 mm; (3) the residual lateral displacement upon wall testing. At the start of the cyclic testing, the lateral displacement at different heights was set to zero. At the peak of the first cycle with 135 mm movement of the loading actuator, the wall deflected significantly to the loading direction (shown in Fig. 12(c)), as characterized by 112.5 mm displacement at the wall's middle, −39.9 mm displacement at the wall's top, and 20.9 mm displacement at the wall's bottom. The positive value indicates the displacement to the loading direction, while the negative value indicates the displacement to the opposite direction. The peak displacement recorded using a set of LVDTs located at the counter-part side of the loading actuator (112.5 mm) which was 22.6 mm smaller than the actuator movement (135 mm) that indicated the wall had compressive deformation in the out-of-plane direction. After removing the lateral loads, the deflection recovered slightly but did not return to zero. At the end of cyclic loading of *Stage II*, the residual lateral displacements were −19.3 mm, 54 mm and 6.9 mm for the top, middle and bottom of the tyre wall, respectively.

3.2.9. Axial displacement during cyclic testing

Fig. 20 shows the axial displacement plotted against drift ratio and lateral displacement for all loading cycles in *Stage II,* with positive axial displacement values indicating compressive deformation of the wall. During each cycle, the height of the wall increased with the increasing lateral displacement and reduced when unloaded. The change in the wall's height mainly resulted from the wall's deflection and gap opening at the wall's mid height. The cumulative residual settlement versus imposed lateral displacement is presented in Fig. 21. The axial displacement at the point of zero lateral displacement at the end of each cycle, was considered as the residual settlement. As shown in Fig. 21., as a general trend the residual settlement increased with the progressively increased amplitude of cycle. The wall settled about 17.0 mm throughout this stage of testing.

3.3. Stage III: Effect of axial compressive loads on the out-of-plane performance of tyre wall

Since the tyre wall had gone through *Stage II* load cycles before *Stage III*, the energy dissipation performance could be largely affected (due to the permanent deformation). Therefore, only the stiffness and force–displacement responses were compared and discussed. At the end of *Stage II* testing, due to changes in applied axial compressive force, the residual lateral displacement reduced from 75 mm to 60 mm at the wall's mid-height. Fig. 22 demonstrates the lateral force–displacement

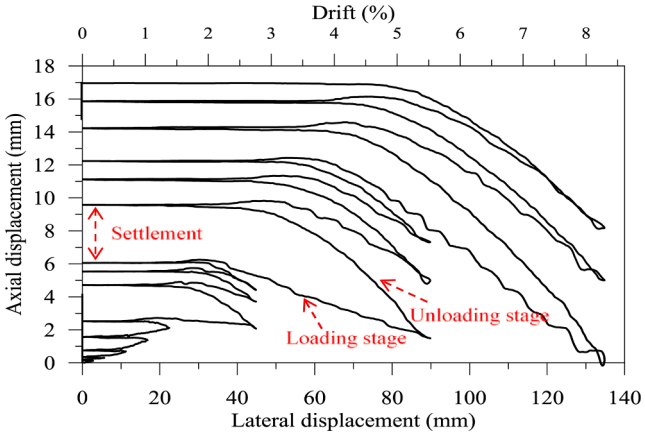

Fig. 20. Axial displacement versus lateral displacement.

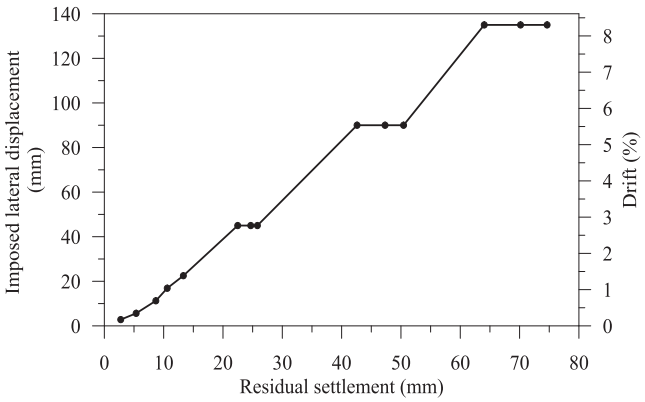

Fig. 21. Imposed lateral displacement versus residual settlement.

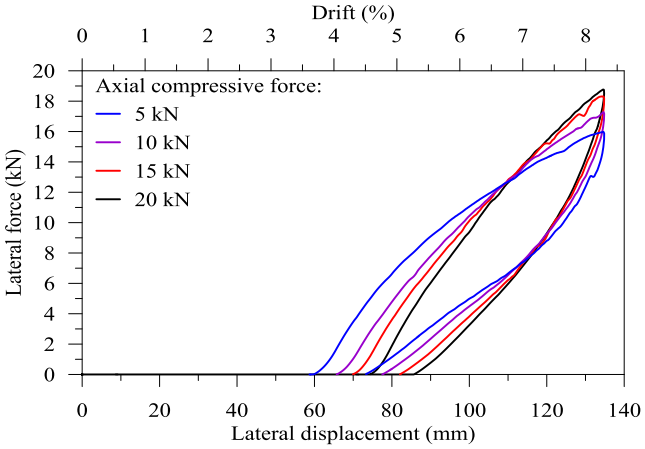

Fig. 22. Lateral force versus lateral displacement (*Stage III*).

results of the tyre wall in *Stage III* testing. From the results, it can be seen that the peak lateral forces increased by 17.5% from 16.0 kN to 18.8 kN when the axial compressive force was four times higher from 5 kN to 20 kN. Fig. 23 presents the relative stiffness versus effective displacement of the wall at different cycles of *Stage III* testing. The effective displacement was computed as the amount of displacement of each cycle after which the lateral force increases from zero. The relative stiffness was calculated as the slope of the line passing through the origin of each cycle (zero force) and the intersection with the force–displacement loop. The

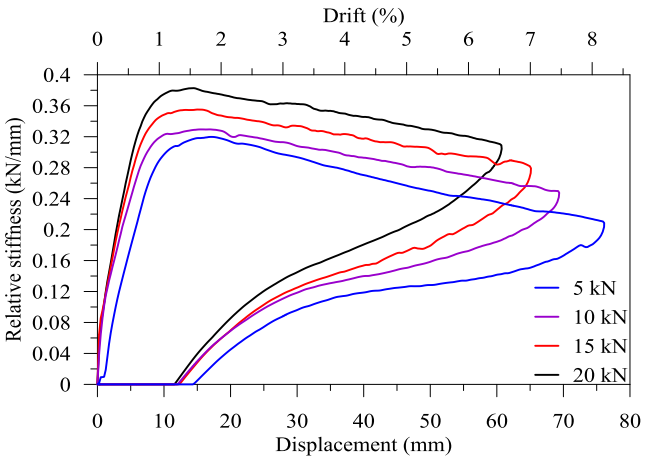

Fig. 23. Relative stiffness versus the effective displacement within the current cycle (*Stage III*).

relative stiffness was not highly sensitive to the axial compressive forces on the wall between 5 kN and 20 kN. By increasing the axial compressive force from 5 kN to 20 kN, the ultimate relative stiffness increased by 23% from 0.31 kN/mm to 0.38 kN/mm. This indicates that that the effect of axial load on the lateral load capacity of the wall is not significant. Therefore, an almost linear relationship between the maximum level of axial load and the lateral capacity of the system can be considered for these ranges of axial loads.

4. Analytical calculation of the test tyre wall

Tyre walls and masonry walls both consist of wall units and can have similarity in their general behaviour and failure pattern. However, the inherent differences between these two systems need to be considered. In masonry walls, there are three typical failure scenarios: tensile cracking at the bedding-joint due to flexural tensile stresses [57]; compression crushing of the masonry units due to the axial load and bending moment [63]; and ultimate instability of the masonry due to large deformation [64].

For tyre walls with large thickness, tensile cracking failure is not a possible mode of failure. To fail in compression, a significant amount of force needs to be applied to the tyre wall which is often much larger than the expected loads in building structures. Experiments performed by Indraratna, Sun [19] revealed that tyre-encased soil could take compressive stress of more than 6500 kPa without failure. Moreover, once a TESE unit is under large bending moment, instead of failure and rupture of the tyre, the encased soil of the compression zone moves towards the tensile zone, which may result in gradual reduction of the stiffness of the wall. It is also worth mentioning that shear failure of TESE unit is also not possible due to the same reason. Unlike masonry walls, shear and flexural cracking failure due to the damage of segmental units is an unlikely failure mechanism in tyre wall systems; instead instability of the wall governs the failure. The failure modes of instability can be expressed as collapse of the wall when its flexural deflection exceeded its point of instability [58,65], beyond which the centre of the axial load moves outside the wall's cross-section, meanwhile the restoring moment is no longer enough to resist the overturning of wall sections. Ultimately, falling of segmental units may occur, especially in the cases when the bond strength in between the segmental units is low.

As observed in the test, the failure of the tyre wall at the ultimate limit state appeared to be due to instability when large deformation occurred at the wall mid-height. In the following, analytical calculations are provided for computing the out-of-plane resistance based on three different scenarios for the instability mechanism: (1) Flexural instability; (2) Sliding instability; (3) Overturning instability. The minimum out-of-plane resistance from these three failure modes can be considered as the lateral capacity of the wall to be compared with the experimental result.

4.1. Flexural instability

Rigid body analysis can be used to determine the flexural instability of the walls. The model assumes that gap opening occurs at mid-height, forming two rigid bodies rotating at the point of lateral load as shown in Fig. 24 (a). The out-of-plane resistance of the wall is governed by the restoring moment due to the wall's self-weight and the applied axial force. By taking the moment about the point of lateral loading, the reaction force at the top, $R_{t,i}$, bottom support $R_{b,i}$, can be expressed as,

$$R_{t,i} = R_{b,i} = \frac{t}{h}\left(P + \frac{W}{2}\right) \tag{3}$$

where, P is the external axial compressive force; W is the wall's self-weight; t is the wall's thickness; and h is the distance between reaction supports. The out-of-plane resistance due to flexural instability (F_i) can be obtained as the sum of $R_{t,i}$ and $R_{b,i}$,

$$F_i = \frac{t}{h}(2P + W) \tag{4}$$

For the test wall, $P = 11.4$ kN (including the self-weight of the loading beam); $W = 35.8$ kN; $t = 570.7$ mm; and $h = 1651.6$ mm. Substituting these values in Eq. (4), the out-of-plane resistance of the tyre wall was calculated as 20.25 kN. This value is only slightly higher than the values obtained from the experiment (19.8 kN). The behaviour of the wall in terms of the rotation of the two halves of the wall around the loading point was also the same. It can be concluded that the rigid body analysis predicts the ultimate out-of-plane resistance of the tyre wall reasonably accurately.

4.2. Sliding instability

The maximum sliding resistance of tyre courses can be calculated using the frictional force at the interface of tyre courses. Therefore, the sliding resistance of the wall, F_s, is a function of the interlocking strength

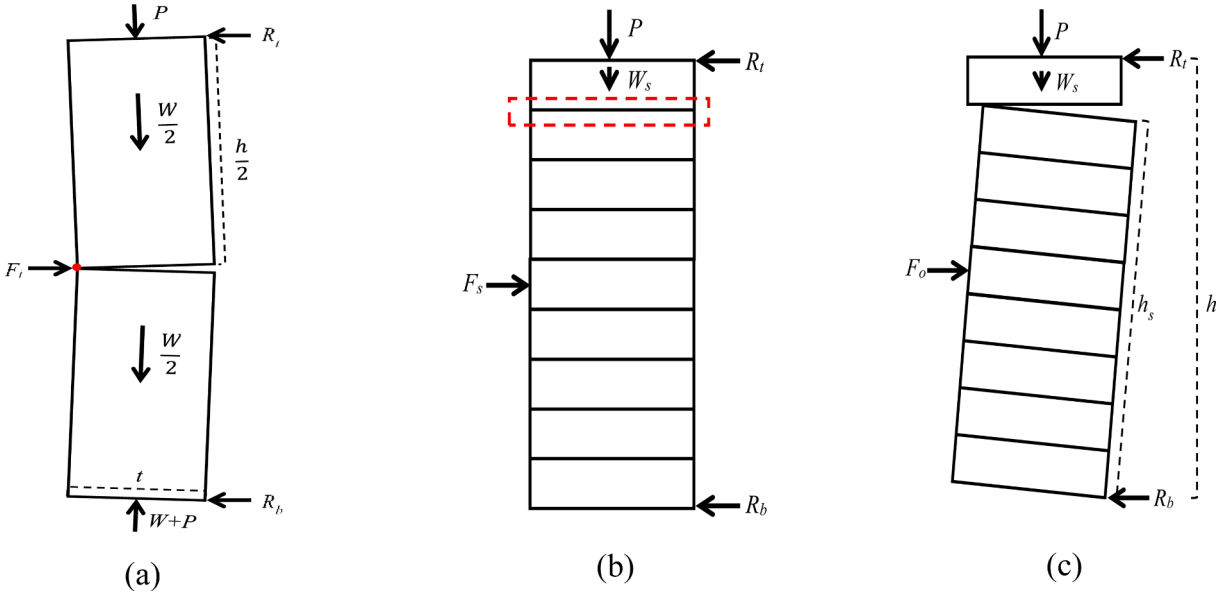

Fig. 24. Possible out-of-plane failure modes in tyre walls: (a) Flexural instability; (b) Sliding instability; (c) Overturning instability.

between tyre courses, frictional coefficient, and the compressive forces at the failure interface, and can be as taken as,

$$F_s = 2 \times [c + \mu(W_s + P)] \quad (5)$$

where, c is the interlocking strength between courses of elements; μ is the frictional coefficient between courses of elements; and W_s is the weight of the wall's portion above the failure interface.

The interlocking strength (c) was tested to be between 1 and 2 kN, while the frictional coefficient (μ) reported by [39] and [40] was in the range of 0.55 to 0.88. The interlocking strength (c) and frictional coefficient (μ) can be obtained by performing a series of direct shear tests. In the direct shear tests, two TESEs were stacked together in a column. One was fully restrained while the other received normal as well as a shear load. The shear force that mobilised the non-fully restrained TESE was regarded as the interlocking strength. The frictional coefficient was the ratio of the normal force to the shear force. The interface between the top two courses of tyres can be considered as the weakest interface in terms of sliding capacity, as shown in Fig. 24 (b), due to the lower applied axial force at this interface. The self-weight of the wall portion above the failure interface was 4 kN (=self-weight of a single course of tyre). Substituting these values in Eq. (5), the out-of-plane resistance due to sliding instability, F_s, was calculated to be in the range of 18.9 kN to 31.3 kN. These values are close to the flexural capacity of the wall (which was 19.8 kN), but sliding failure did not occur. Note that while the values of c and μ were calculated for pure sliding of individual tyres on each other, a higher range of these values seems to be applicable to the wall members. This can be due to the behaviour of the wall where shear capacity is coupled with flexural deformation. As shown in Fig. 12, there might be some level of arching action on the wall when the wall gap opening occurs at the mid-height. This mechanism can improve the shear capacity of the wall, which needs to be considered in the calculations.

4.3. Overturning instability

For a wall constructed with courses of individual elements without using bonding materials, once the lateral force reaches the sliding resistance (as presented in Section 4.2), the segmental wall may fail in a combined sliding and flexural instability mechanism in a manner of overturning as shown in Fig. 24(c). Assuming that the wall rotates about the point of bottom reaction support, the out-of-plane overturning resistance, F_o, can be calculated as

$$F_o = \frac{(P + W)t + 2f_s h_s}{h} \quad (6)$$

where f_s is the frictional resistance at the sliding interface (=half of F_s as calculated using Eq. (5)) and h_s is the distance between the failure interface and the bottom rotation point.

By substituting the parameters of the test ($P = 11.4$ kN, $W = 35.8$ kN, $t = 570.7$ mm, f_s ranged from 7.15 kN to 11.25 kN, h_s=1548.3 mm, h=1651.5 mm), the out-of-plane overturning resistance, F_o, was calculated to be in the range of 34.0 to 45.4 kN.

Out of the three modes of instability failure, the minimum capacity was obtained as the flexural instability condition. Based on the results of this study, it is suggested that Eq. (4), 5 and 6, be used to determine the lateral capacity of the tyre wall based on flexural instability, sliding stability and overturning instability, and the lowest of which be considered as the lateral capacity of the tyre wall.

5. Conclusions

This research attempted to understand the axial and lateral behaviour of tyre walls suitable for earth-sheltered housing such as Earthships. To achieve that, a test tyre wall was designed, constructed and tested in three stages. The axial force–displacement performance of tyre wall subjected to dead load from a light-weight roof was investigated in the first stage. The lateral performance of the tyre wall subjected to combined compressive load and the cyclic out-of-plane load was studied in the second stage. The effect of axial compressive load on the out-of-plane performance was examined in the third stage. Moreover, analytical approaches were proposed to predict the out-of-plane lateral resistance of tyre walls. The outcomes of this investigation are summarised below:

- The test tyre wall provided the required strength to support a light-weight roof while going through a settlement of 0.2% of height. The axial force–displacement relationship could be approximated as linear and can be used to calculate the tyre wall's settlement at different axial load. The test results indicated that a tyre wall could be used as an axial load-bearing structural member in residential housing constructions. Further study should be carried out to investigate the axial strength capacity of tyre wall for axial limit state design purposes, especially more slender walls with a higher number of courses which are prone to buckling.
- The failure of tyre walls subjected to combined compressive and out-of-plane loads was mainly characterized by sliding and the joint rotation opening mechanism at the wall's mid-height. The 'fat' lateral force–displacement hysteresis loops demonstrate the tyre wall's out-of-plane performance to be highly inelastic, which is beneficial with regard to its seismic performance. The energy dissipation mainly resulted from the residual lateral displacements and the frictional resistance.
- An increase in axial force from 5 kN to 20kN improved the tyre wall's ultimate out-of-plane load by 17.5% and improved relative stiffness by 23%, while the residual displacement was reduced by 20%. This indicates that for common gravity roof loads the axial stress would have a slight influence on the out-of-plane performance. It is also concluded that even a light-weight roof placed on the tyre wall can improve the integrity of the wall and induce the wall additional capacity to carry the lateral loads due to wind, earthquake and soil pressure.

The analytical results were consistent with the observed tyre wall's performance. The analytical approach presented in this study, which was based on an instability mechanism, can potentially be adopted to calculate the capacity of tyre walls and aid in the engineering of such structures.

This study investigated the structural performance and design method of load-bearing wall built of tyre-encased-soil elements (TESEs). It provided scientific evidence to safely and systematically design tyre walls for single-story, earth-sheltered (or non-earth-sheltered) residential housing purposes. It is anticipated that this may offer some assurance and evidence to built environment professions, i.e., regulators, standards committees, engineers, architects, certifiers, builders and potential homeowners, regarding the structural integrity of tyre walls. The tyre wall as tested and presented in this paper is the first of its kind that has been scientifically tested and studied in terms of the factors studied in this paper. Further studies should include experimental and numerical studies on full-scale tyre walls to obtain more data for further verifying the analytical equation and to conduct parametric analysis for quantifying the influence of factors such as tyre size/type, encased materials and dynamic actions on the tyre wall structural performance.

CRediT authorship contribution statement

Yachong Xu: Writing – original draft, Writing – review & editing, Methodology, Investigation, Formal analysis. **Martin Freney:** Writing – review & editing, Funding acquisition. **Reza Hassanli:** Writing – review & editing, Methodology. **Yan Zhuge:** Writing – review & editing. **Md. Mizanur Rahman:** Writing – review & editing. **Md. Rajibul Karim:** Writing – review & editing.

Declaration of Competing Interest

The authors declare that they have no known competing financial interests or personal relationships that could have appeared to influence the work reported in this paper. Dr. Martin Freney operates a company that provides architectural services for the design of Earthship homes.

Acknowledgment

The authors would like to acknowledge the University of South Australia and the industry partners Tyre Stewardship Australia and Tyrecycle Pty. Ltd for the research scholarship funding and the donation of tyre materials respectively. The authors thank Mr. T. Golding, Mr. I. Whitehead, Dr. H. Senko, Mr. G. ONeil, Mr. R. Muscher and Mr. C. Sweetman, for technical assistance when preparing and testing the tyre wall. The authors also acknowledge the contribution of the following master's final year students who assisted in the experimental work reported in this paper: Mr. J. K. Piprotar, Mr. A. Kansari, Mr. J. L. Changani and Mr. B. S. Viradiya. The authors also thank Mr. T. Ha and Mr. S. Plummer of MLEI Consulting Engineers for their support as the industry experts.

References

[1] Gilson D. Annual Report 2016/2017. Tyre Stewardship Australia; 2017.
[2] Bianco I, Panepinto D, Zanetti M. End-of-life tyres: comparative life cycle assessment of treatment scenarios. Appl Sci 2021;11(8):3599. https://doi.org/10.3390/app11083599.
[3] Ben Hassine W, Hassis H, Ben Hamida A. An extension, flexural, and warping model of soil reinforced by used tire's portions related by linear inclusion. Eur J Mech A Solids 2005;24(4):630–43.
[4] Anderson M, Hatherly I. Tyre disposal sites in the West Midlands region of the UK as mosquito breeding sites. International pest control 2009;51(4):187–8.
[5] Reschner K. Scrap tire recycling, A summary of prevalent disposal and recycling methods. Entire-Engineering, Berlin 2008;1:115–240.
[6] Takallou H, Hicks G, Takallou M. Use of rubber modified asphalt for snow and ice control. VTI Rapport 1990.
[7] Li D, Zhuge Y, Gravina R, Mills JE. Compressive stress strain behavior of crumb rubber concrete (CRC) and application in reinforced CRC slab. Constr Build Mater 2018;166:745–59.
[8] Li D, Zhuge Y, Gravina R, Benn T, Mills JE. Creep and drying shrinkage behaviour of crumb rubber concrete (CRC). Aust J Civil Eng 2020;18(2):187–204.
[9] Hassanli R, Youssf O, Mills JE. Experimental investigations of reinforced rubberized concrete structural members. J Build Eng 2017;10:149–65.
[10] Hassanli R, Youssf O, Mills JE. Seismic performance of precast posttensioned segmental FRP-confined and unconfined crumb rubber concrete columns. J Compos Constr 2017;21(4):04017006. https://doi.org/10.1061/(ASCE)CC.1943-5614.0000789.
[11] Huat BBK, Aziz AA, Chuan LW. Application of scrap tires as earth reinforcement for repair of tropical residual soil slope. Electron J Geotech Eng 2009;13:1–9.
[12] Li L, Xiao H, Zheng J, Chen L, Sun M, Sun L, et al. The model test of waste tire reinforced slope. Gongcheng Lixue/Eng Mech 2015;32:79–85.
[13] Li L, Xiao H, Ferreira P, Cui X. Study of a small scale tyre-reinforced embankment. Geotext Geomembr 2016;44(2):201–8.
[14] Li L, Shi A, Zhang L, Xiao H, Jiang M. Experimental investigations on the mechanically stabilised earth wall under static load conditions. Eur J Environ Civil Eng 2021;25(4):575–98.
[15] Garga VK, O'Shaughnessy V. Tire-reinforced earthfill. Part 1: Construction of a test fill, performance, and retaining wall design. Can Geotech J 2000;37:75–96.
[16] O'Shaughnessy V, Garga VK. Tire-reinforced earthfill. Part 2: Pull-out behaviour and reinforced slope design. Can Geotech J 2000;37:97–116.
[17] Long N-T. Utilization of used tyres in civil engineering-the Pneusol'Tyresoil. Environ Geotech 1996:809–14.
[18] Yoon YW, Heo SB, Kim KS. Geotechnical performance of waste tires for soil reinforcement from chamber tests. Geotext Geomembr 2008;26(1):100–7.
[19] Indraratna B, Sun Q, Grant J. Behaviour of subballast reinforced with used tyre and potential application in rail tracks. Transp Geotech 2017;12:26–36.
[20] Sun Q, Indraratna B, Heitor A. Behaviour of a capping layer reinforced with recycled tyres. Proc Inst Civil Eng – Ground Improv 2019;172(3):127–37.
[21] Reynolds M. Earthship volume 1: how to build your own. Taos: Solar Survival Press; 1990.
[22] Freney M, Soebarto V, Williamson T. Earthship monitoring and thermal simulation. Arch Sci Rev 2013;56(3):208–19.
[23] Freney M. Earthship eco homes, self sufficient & sustainable; <https://www.earthshipecohomes.com.au/>2015 (accessed 23/06/2021).
[24] Indraratna B, Sun Q, Heitor A, Grant J. Performance of rubber tire-confined capping layer under cyclic loading for railroad conditions. J Mater Civ Eng 2018;30(3):06017021. https://doi.org/10.1061/(ASCE)MT.1943-5533.0002199.
[25] Li LH, Tang HM, Xiao BL. Discarded tire implications in reinforced slope. Adv Mater Res 2012;374-377:1430–3.
[26] Li L, Cui F, Xiao H, Ma Q, Qin L. Shear performance of waste tires, geogrid and geocell reinforced soils. In: Li L, Cetin B, Yang X, editors. Proceedings of GeoShanghai 2018 international conference: ground improvement and geosynthetics. Singapore: Springer Singapore; 2018. p. 463–72. https://doi.org/10.1007/978-981-13-0122-3_51.
[27] Li L, Cui F, Ferreira P, Xiao H, Jie H. Experimental study of embankments with different reinforcement materials and spacing between layers. Geotext Geomembr 2019;47(4):477–82.
[28] Reynolds M. Earthship Academy Haiti, <https://www.earthshipglobal.com/haiti> (accessed 22/06/2021).
[29] Leeor A. Earthship Karuna | A self sufficient and sustainable off-grid passive solar home. <https://www.earthshipkaruna.net/> (accessed 23/06/2021).
[30] Ip K, Miller A. Thermal behaviour of an earth-sheltered autonomous building – the Brighton Earthship. Renew Energy 2009;34(9):2037–43.
[31] Freney M, Soebarto V, Williamson T. Thermal comfort of global model Earthship in various European climates. Proceedings of BS2013: 13th Conference of International Building Performance Simulation Association, Chambéry, France, August 26-28, 2013: pp.1625-1632.
[32] Temple EK, Rose E. Sustainable construction in rural Guatemala. Arch Dis Child 2011;96(11):1048–51.
[33] Grindley PC, Hutchinson M. The thermal behaviours of an earthship. Renewable Energy 1996;8(1-4):154–9.
[34] Edun A, Hachem-Vermette C. Energy and environmental impact of recycled end of life tires applied in building envelopes. Journal of Building. Engineering 2021;39:102242. https://doi.org/10.1016/j.jobe.2021.102242.
[35] Freney MHP. Earthship architecture: post occupancy evaluation, thermal performance & life cycle assessment. Adelaide, Australia: The University of Adelaide; 2014.
[36] Freney M, Soebarto V, Williamson T. Learning from 'Earthship'based on monitoring and thermal simulation. In: 46th annual conference of the architectural science association (ANZAScA). Griffith University; 2012.
[37] Paschich E, Hendricks P. The tire house book. Sunstone Press; 1995.
[38] Hewitt M, Telfer K. Earthships in Europe. IHS BRE Press 2012.
[39] Griepentrog TE. Engineering evaluation of, earth-filled tire construction, Dennis Weaver Residence, Ridgway, Colorado. Buckhorn Geotech; 1990.
[40] Zimmerman A, Burger E, Nolan J. Testing and analysis of modified rammed earth tyre walls. E90 Project: Swarthmore College; 2011.
[41] Standards Australia. AS 1289.3.6.1-2009, Methods of testing soils for engineering purposes – Soil classification tests – Determination of the particle size distribution of a soil - Standard method of analysis by sieving. Australia: Standards Australia Limited; 2009.
[42] ASTM International. ASTM D2487-11, Standard practice for classification of soils for engineering purposes (Unified Soil Classification System). West Conshohocken, PA: ASTM International; 2011.
[43] Standards Australia. AS 1289.5.1.1, Methods of testing soils for engineering purposes - Soil compaction and density tests—Determination of the dry density/moisture content relation of a soil using standard compactive effort. Australia: Standards Australia Limited; 2017.
[44] Baranowski P, Małachowski J, Mazurkiewicz Ł. Local blast wave interaction with tire structure. Defence Technol 2020;16(3):520–9.
[45] Baranowski P, Malachowski J, Mazurkiewicz L. Numerical and experimental testing of vehicle tyre under impulse loading conditions. Int J Mech Sci 2016;106:346–56.
[46] Baranowski P, Malachowski J, Janiszewski J, Wekezer J. Detailed tyre FE modelling with multistage validation for dynamic analysis. Mater Des 2016;96:68–79.
[47] Baranowski P, Janiszewski J, Małachowski J. Tire rubber testing procedure over a wide range of strain rates. J Theor Appl Mech 2017;727.
[48] ASTM International. ASTM D4885, Determining Performance Strength of Geomembranes by the Wide Strip Tensile Method. West Conshohocken, United States: ASTM International; 2018.
[49] ASTM International. ASTM D4595, tensile properties of geotextiles by the wide-width strip method. West Conshohocken, United States: ASTM International; 2011.
[50] ASTM International. ASTM D638-14, Standard test method for tensile properties of plastics. West Conshohocken, PA: ASTM International; 2014.
[51] Australian Building Codes Board. National construction code 2019 – building code of Australia – volume two. Canberra, ACT, Australia: Australian Building Codes Board; 2019.
[52] Ghobarah A, El Mandooh Galal K. Out-of-Plane Strengthening of Unreinforced Masonry Walls with Openings. J Compos Constr 2004;8(4):298–305.
[53] ASTM International. ASTM E2126-11, Standard test methods for cyclic (reversed) load test for shear resistance of vertical elements of the lateral force resisting systems for buildings; 2011.
[54] Coulbourne Consulting. Residential structural design guide, A state-of-the-art engineering resource for light-frame homes, apartments, and townhouses; 2017.
[55] Standards Australia. AS/NZS 1170.1:2002, Structural design actions, Part 1: Permanent, imposed and other actions. Australia: Standards Australia Limited; 2002.
[56] Wang J, Heath A, Walker P. Experimental investigation of brickwork behaviour under shear, compression and flexure. Constr Build Mater 2013;48:448–56.
[57] Derakhshan H, Griffith MC, Ingham JM. Airbag testing of multi-leaf unreinforced masonry walls subjected to one-way bending. Eng Struct 2013;57:512–22.
[58] Willis CR. Design of unreinforced masonry walls for out-of-plane loading. Adelaide, Australia: The University of Adelaide; 2004.

[59] Doherty KT. An investigation of the weak links in the seismic load path of unreinforced masonary buildings. Australia: The University of Adelaide; 2000.
[60] ASCE. Prestandard and commentary for the seismic rehabilitation of buildings: FEMA 356. Washington, D.C., US: American Society of Civil Engineers; 2000.
[61] Standards Australia. AS 1170.4:2007, Structural design actions, Part 4: Earthquake actions in Australia. Australia: Standards Australia Limited; 2007.
[62] Chopra AK. Dynamics of Structures: Theory and applications to earthquake engineering. 5th ed. Prentice Hall/ Pearson; 2019.
[63] Javadi M, Hassanli R, Rahman MM, Karim MR. Experimental study on cyclic behavior of post-tensioned segmental retaining walls (PSRWs). Eng Struct 2021; 229:111619. https://doi.org/10.1016/j.engstruct.2020.111619.
[64] Al-Fakih A, Mohammed BS, Wahab MMA, Liew MS, Mugahed Amran YH. Flexural behavior of rubberized concrete interlocking masonry walls under out-of-plane load. Constr Build Mater 2020;263:120661. https://doi.org/10.1016/j.conbuildmat.2020.120661.
[65] Griffith MC, Lam N, Wilson J. Displacement-based assessment of the seismic capacity of unreinforced masonry walls in bending. Aust J Struct Eng 2006;6(2): 119–32.